Electron-Nanobunch-Width-Dominated Spectral Power Law for Relativistic Harmonic Generation from Ultrathin Foils

Matthew R. Edwards,[1,2,*] Nicholas M. Fasano,[1] and Julia M. Mikhailova[1,†]
[1]Department of Mechanical and Aerospace Engineering, Princeton University, Princeton, New Jersey 08544, USA
[2]Lawrence Livermore National Laboratory, Livermore, California 94550, USA

(Received 10 May 2019; revised manuscript received 10 February 2020; accepted 6 April 2020; published 7 May 2020)

Relativistic high-order harmonic generation from solid-density plasma offers a compact source of coherent ultraviolet and x-ray light. For solid targets much thinner than the laser wavelength, the plasma thickness can be tuned to increase conversion efficiency; a reduction in total charge allows for balancing the laser and plasma driving forces, producing the most effective interaction. Unlike for semi-infinite plasma surfaces, we find that for ultrathin foil targets the dominant factor in the emission spectral shape is the finite width of the electron nanobunches, leading to a power-law exponent of approximately $10/3$. Ultrathin foils produce higher-efficiency frequency conversion than solid targets for moderately relativistic ($1 < a_0 < 40$) interactions and also provide unique insight into how the trajectories of individual electrons combine and interfere to generate reflected attosecond pulses.

DOI: 10.1103/PhysRevLett.124.185004

The extreme electric and magnetic fields present at the focus of petawatt-class lasers and the massive net Coulomb forces in solid-density plasmas can produce relativistic electrons in femtoseconds. Electrons accelerated by a relativistic-intensity laser pulse focused on a solid will radiate broadband high-frequency light, creating a compact brilliant x-ray source [1–8]. Ionized interaction media support far higher laser intensities than gas-based high-order-harmonic generation (HHG), and relativistic HHG offers a route to high-energy attosecond pulses, attosecond pump-probe spectroscopy, and x-ray nonlinear optics [9–11]. In the coherent synchrotron emission (CSE) model of HHG from relativistic plasma mirrors, a dense electron bunch is driven in an instantaneously circular trajectory at the plasma surface during each laser cycle, emitting synchrotron-like radiation with a power-law spectrum [12,13]. The CSE model predicts that the spectral energy scales with harmonic frequency (ω) as $\omega^{-4/3}$ up to a cutoff ω_γ which depends on the maximum Lorentz factor (γ) [12]. Relativistic HHG varies with the laser intensity, plasma density profile [14–17], angle of incidence [18,19], and the frequency composition [20–23], pulse duration [24], and polarization [25] of the driving light. Additionally, the dynamics will change as the target thickness (d) is reduced—previous work falls in three regimes: semi-infinite ($d \gg \lambda$) [1,2,19,26–29], thin ($d \approx \lambda$) [25,30–38], and ultrathin ($d \ll \lambda$) [13,32,39–43], where λ is the laser wavelength—with thin and ultrathin targets allowing for the collection of both transmitted and reflected harmonics. Although semi-infinite and thin targets behave similarly for few-cycle driving pulses, nanometer-scale foils ($d \ll \lambda$) enter a different regime, allowing high efficiency, and, as we demonstrate here, showing behavior that can be explained by a modified CSE mechanism.

We find that for ultrathin targets the spectrum of the reflected radiation can be approximated as a power law $I(\omega) = \omega^{-p}$ with $p = 10/3$ up to a cutoff at $\omega_\gamma = \sqrt{8\alpha_1}\gamma_z^3$. This scaling arises because although individual electrons follow synchrotron-like trajectories and produce $\omega^{-4/3}$ CSE spectra, emission events for ultrathin targets are spread broadly in time and space, limiting the fraction of electrons that constructively interfere. The distribution of high-frequency generation events has a sharp leading edge and can be approximated by a step function; only electrons within a half-wavelength of this edge coherently add, leading to an additional factor ω^{-2} in the spectrum. This analysis of the finite bunch width extends to semi-infinite targets, explaining apparent spectral cutoffs at frequencies much lower than those predicted by the CSE model.

Consider an ultrathin ($D = d/\lambda \ll 1$) overdense plasma ($N = n_e/n_c > 1$, $n_c = m_e\omega_L^2/4\pi e^2$) in a relativistic ($a_0 = eE/m_e\omega_L c > 1$) laser field as illustrated in Fig. 1(a), where E is the maximum laser electric field, $\omega_L = 2\pi c/\lambda$ is the frequency, n_e is the electron number density, and e and m_e are the electron charge and mass. For $a_0 \gg 1$, the trajectories of plasma electrons depend on $S = N/a_0$, not either a_0 or N separately [20,44]. In the limit $D \to 0$, with D much smaller than any other length scale, the total charge in the foil rather than the exact initial distribution governs the interaction. The characteristic parameter SD—the total charge reduced by a relativistic factor [39,45]—describes the effective plasma thickness, and the parametric dependence of the efficiency (η) simplifies:

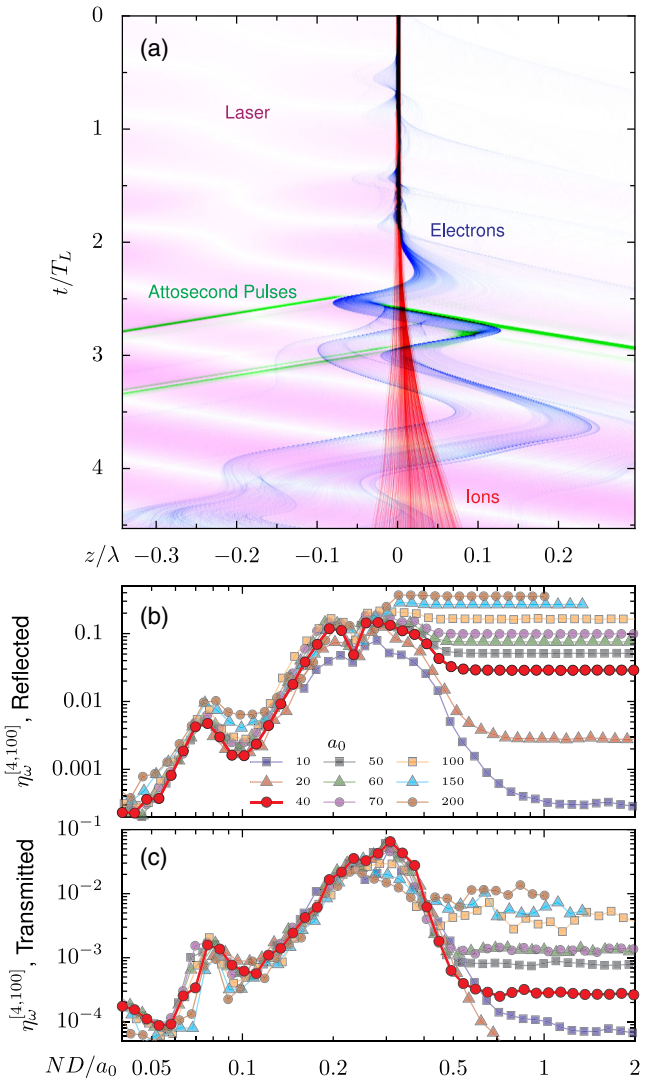

FIG. 1. Simulations of relativistic HHG. (a) Plot of electron density (blue), ion density (red), laser magnetic field (purple) and attosecond pulses (green) in space and time for $a_0 = 20$, $N = 500$, $D = 0.005$, and $\theta_L = 30°$. Efficiency ($\eta_\omega^{[\omega_{LF},\omega_{UF}]}$ is the fraction of incident energy produced with $\omega_{LF} < \omega < \omega_{UF}$) of reflected (b) and transmitted (c) harmonic generation for varied SD, a_0, and D at $N = 400$ and $\theta_L = 30°$.

$$\eta = f(N, a_0, D, \ldots) = f\left(\frac{ND}{a_0}, \ldots\right). \tag{1}$$

In Figs. 1(b) and 1(c) the efficiency of harmonic conversion to the interval $4 < \omega/\omega_L < 100$ in both the reflected (b) and transmitted (c) directions collapses to a single line for $SD < 0.2$.

The utility of ultrathin foils arises from the collapse to ND; changing thickness adjusts the effective density of the target. Relativistic HHG is most efficient when the laser and plasma forces are balanced, i.e., $a_0/N \approx 0.5$ [22], which is difficult to achieve for solid densities ($N \approx 400$) with current laser intensities, so reducing the effective N with small D is a route to more efficient harmonic conversion. The efficiency peak for the $a_0 = 40$ line in Figs. 1(b) and 1(c) shows that optimal ultrathin foils are a more efficient source for both reflected and transmitted harmonics than semi-infinite targets at moderate intensity. Note that the interval $4 < \omega/\omega_L < 100$ spans the plasma frequency, so for $SD > 1$, transmitted harmonics with $\omega/\omega_L < \sqrt{N} = 20$ are filtered by the plasma. We must carefully distinguish micron-scale (thin) targets ($D \approx 1$)—which for few-cycle lasers will behave similarly to semi-infinite targets due to the finite speed of light—from nanometer-scale (ultrathin) targets ($D \ll 1$), where the finite plasma extent fundamentally affects the interaction. In addition to increased efficiency, for ultrathin foils the entire phase-space distribution can be adequately represented with relatively few particles (<10 000); the detailed trajectory of every particle can be recorded to build a complete picture of the contributions to the total spectrum.

Using one-dimensional particle-in-cell (PIC) simulations (BOPS [46] and EPOCH [47]) with resolutions between 2 500 and 50 000 cells/λ and 50–10 000 particles/cell, we simulated relativistic HHG for ultrathin targets with varied a_0, N, D, and angle of incidence (θ_L). We emphasize single-cycle driving pulses since the high-frequency emitted pulses are formed in a fraction of a cycle and the number of cycles which efficiently drive harmonics tends to be limited even for longer (> 20 fs) pulse duration by the breakup of thin foils [48]. To analyze the spectral contributions of individual electrons, we note that in one dimension the propagating (transverse) electric field produced by a charged plane may be written [50]:

$$E_y = 2\pi\sigma \frac{\beta_y}{1 - \beta_z \mathrm{sgn}(z - z_u)}, \tag{2}$$

where $\beta_{y,z}$ are the y and z velocity components normalized by c, z is the plane position, σ is the charge density, and z_u is the observation location. To address reflection, we choose z_u such that $z_u < z$ for all particles and time and Eq. (2) simplifies to $E_y = (2\pi\sigma)\beta_y/(1 - \beta_z)$. The nonlinearity that distinguishes this process from simple reflection (where $\beta_z = 0$ and $\beta_y \propto \sin\omega t$) arises from both the nonsinusoidal behavior of β_y for relativistic fields and the nonzero value of β_z, initially driven by the laser magnetic field.

Figure 2 shows the detailed electron motion during the generation of an attosecond pulse over a single optical half-cycle. The blue-to-red lines in each subplot of Fig. 2 correspond to evenly distributed electron trajectories, with colors ordered by emission arrival time. Most electrons follow synchrotron-like trajectories [Fig. 2(a) inset], emitting high-frequency radiation when their velocities point toward $-z$. This emission time matches a peak in the Lorentz factor in the reflected direction ($\gamma_z = 1/\sqrt{1 - v_z^2/c^2}$), plotted in Fig. 2(a) against the advanced time ($t_a = t + z/c$) to directly

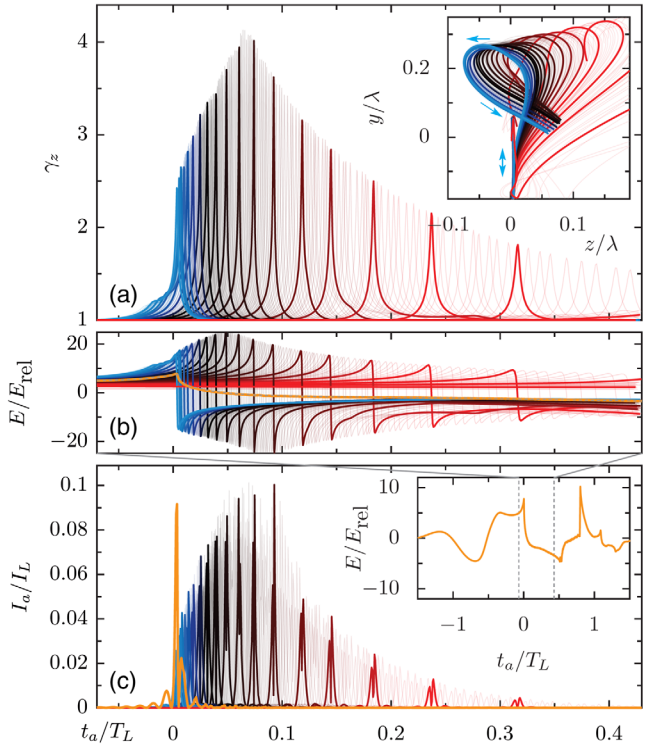

FIG. 2. Contribution of individual electrons at $a_0 = 10$, $N = 500$, $\theta_L = 0°$, and $D = 0.004$. (a) The Lorentz factor in the direction of emission for selected electrons in the advanced time, showing the relatively long spread of emission times. The blue-red color scale marks time of emission and corresponds across plots. Inset: trajectories of selected electrons in the zy plane. (b) The electric field generated by each particle in (a), together with the total field (orange). The fields of individual electrons have been multiplied by the number of electrons. (c) The high-frequency ($\omega/\omega_L > 40$) radiation intensity emitted by selected electrons compared to the total high-frequency intensity (orange). Inset: total reflected electric field. $E_{\rm rel} = m_e\omega_L c/e$.

show when the fields [Fig. 2(b)] produced by particular trajectories arrive at the observation point. The spread of the γ_z peaks over several tenths of a laser cycle results in the distribution of high frequency emitted field components over a scale much longer than their wavelength.

The total field [Fig. 2(b), orange] is the sum of individual electron contributions; it only exhibits a sharp transition near $t_a = 0$, though the individual fields have high-frequency structure for t_a/t_L as large as 0.3. Despite this spread in high frequencies ($\omega/\omega_L > 40$) and the attosecond pulses that would be produced by isolated electrons [Fig. 2(c)], the contributions destructively interfere for $t_a > 0.01T_L$, so the total emission is a single attosecond pulse with duration $\approx T_L/100$. Although most electrons in the plasma are sufficiently relativistic to produce radiation with $\omega/\omega_L > 40$, only the small fraction near the leading edge of the emission contribute constructively to the total spectrum.

Access to the fields produced by individual electrons allows analysis of the individual spectral contributions. In Fig. 3, the spectra resulting from selected trajectories are plotted in comparison to a CSE-type spectrum [12]:

$$I(\omega) \propto |\tilde{f}(\omega)|^2\omega^{-4/3}\left\{\mathrm{Ai}'\left[\left(\frac{\omega}{\omega_\gamma}\right)^{2/3}\right]\right\}^2, \tag{3}$$

which is derived by assuming that the radiation emitted by a charge bunch is dominated by the motion near the time of emission, approximated by $j(t) = \alpha_0 t$ and $z(t) = \beta_z t + \alpha_1 t^3/3$, where α_0 and α_1 are calculated from the bunch trajectory [12]. For a single point particle, the shape function f is $\delta(z)$, leading to a unity factor in the spectrum. If we examine the trajectory of a single electron—here, that with the highest γ_z—and calculate the spectrum, we have excellent agreement to both $p = 4/3$ and the $\omega_\gamma = \sqrt{8\alpha_1}\gamma_z^3$ cutoff, as shown in Fig. 3(a). This holds if we consider, for example, the total spectrum produced by the 5% of electrons closest to the leading edge of the bunch [Fig. 3(b), red], but not for the total spectrum of all electrons (black), which, with ($p \approx 3.3$) follows neither the prediction of CSE nor the $p = 8/3$ of the relativistic oscillating mirror model [5]. Since the spectra produced by individual electrons and small groups of electrons are predictable from the CSE model, deviations from 4/3 scaling could be explained as a violation of the bunching model due to a spread in either γ_z or emission times.

The individual particles which dominate harmonic generation exhibit a relatively narrow distribution in maximum γ_z, suggesting that for ultrathin foils the primary contributor to the disagreement is the lack of coherence due to the finite electron bunch size. In Fig. 3(c), the spectrum produced by adding together the spectral intensities (neglecting phase) of every individual particle (solid red) is almost the same as the spectrum produced by the single fastest particle (blue); both agree reasonably with the calculated CSE spectrum (dashed orange), but fail to match the actual total spectrum (black), which is affected by both spectral intensity and phase.

From Fig. 2(c), we note that the coherent emission comes from the leading edge of the bunch, where the initial half cycle of radiation is not canceled. If we assume that the electron emission times are distributed evenly over a window much longer than the harmonic (n) period, then the number of electrons which will emit coherently scales as λ_n, and the intensity of the emitted harmonic n scales as λ_n^2, or ω^{-2}. This is equivalent to choosing a Heaviside step function as the shape function f in Eq. (3). A Gaussian distribution of electrons would produce an exponential spectrum. Our observation of a power-law spectrum for wavelengths much shorter than the bunch duration highlights the importance of the sharp leading edge.

The additional factor of ω^2 means that up to the cutoff—which remains at ω_γ—the harmonic intensity approximately decreases as:

$$I(\omega) \propto \omega^{-10/3} \tag{4}$$

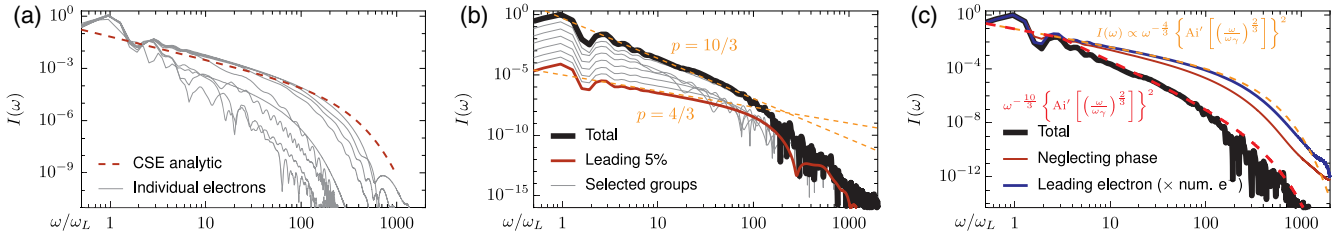

FIG. 3. Relativistic HHG with $a_0 = 10$, $N = 500$, $D = 0.0024$, and $\theta_L = 0°$. (a) The spectra that would be produced by individual electrons compared to an analytic spectrum (dashed red line) calculated using γ_z and α_1 for the highest-γ_z electron. (b) The spectra produced by groups of electrons, progressively increasing from the 5% closest to the front (red) to the entire target (black). The leading edge group produces a $4/3$ spectrum because the component electrons are distributed narrowly and constructively interfere. (c) The total spectrum (black) compared to that of the single highest-γ_z electron (blue) multiplied by the number of electrons and (red) assuming that the unique spectrum from each individual electron is emitted coherently. The relatively small difference between the red and blue lines, in comparison to that between the blue and black lines, suggests that the spectral shape is due to a distribution in emission location rather than in γ_z and α_1. The dashed orange line marks the analytic spectrum, and the dashed red line shows the correction for the finite bunch size.

as long as our assumption about the bunch shape holds. As the spectra in Figs. 4(a) and 4(b) and the fitted values of p in Fig. 4(c) show, ultrathin-foil spectra lie close to $p = 3.3 \pm 0.5$ across a broad range of parameters. Some deviation arises from uncertainty in the power-law fit, which has been marked by error bars for selected points. Although p varies little across the $0.05 < SD < 0.3$ range plotted in Fig. 4(c), Fig. 1(b) shows that the total reflected harmonic signal peaks near $SD \approx 0.2$. For $SD < 0.2$ the total efficiency drops because the plasma is too tenuous to reflect most laser energy; however, the harmonics that are generated follow the same $p \approx 10/3$ scaling law. For $SD \gg 0.2$ and $a_0/N \ll 1$ the interaction is in an inefficient semi-infinite target regime, where the laser is too weak to efficiently drive harmonics. The maximum Lorentz factor produced by ultrathin foils tends to be higher than that for semi-infinite targets; in Fig. 4(d), γ_z for $ND/a_0 = 0.1$ is a larger fraction of a_0 than that for even relatively efficient values of a_0/N, implying a higher limit for the γ_z^3 cutoff.

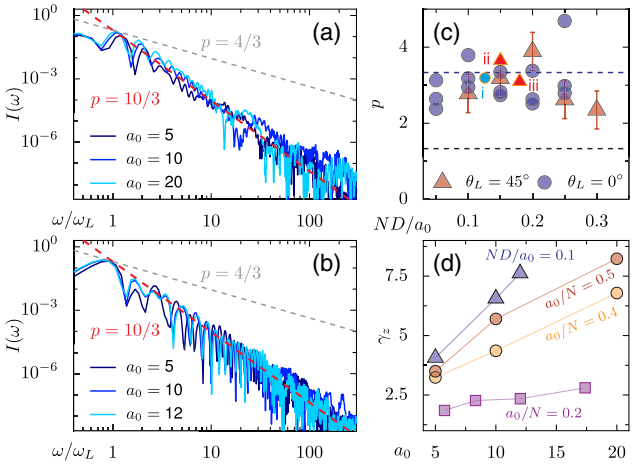

FIG. 4. Spectra of HHG with (a) $\theta_L = 45°$, $S = 100$, $SD = 0.1$, and (b) $\theta_L = 0°$, $S = 100$, $SD = 0.15$ compared to power-law scaling with $p = 4/3$ and $p = 10/3$. (c) The power-law exponent found for varied ND/a_0 for $\theta_L = 0°, 45°$ and $a_0 = 5$, 10, 12, with dashed lines at $p = 4/3$ (CSE) and $p = 10/3$ (CSE with bunch-width modification). Marked points are from multidimensional simulations: (i) 2D, $a_0 = 47.6$, $SD = 0.126$, $\theta_L = 0°$, (ii) 2D, $a_0 = 40$, $SD = 0.15$, $\theta_L = 45°$, (iii) 3D, $a_0 = 20$, $SD = 0.12$, $\theta_L = 45°$. Additional details are in the Supplemental Material [48]. (d) Maximum γ_z against a_0 for both an ultra-thin foil ($ND/a_0 = 0.1$) and selected semi-infinite conditions, all at $\theta_L = 30°$.

The $10/3$ power law also appears in limited parts of the spectra produced by semi-infinite targets, which for efficient values of a_0/N (i.e., $a_0/N \approx 0.5$) follow $p = 4/3$ at lower frequencies. Previous work [12] describes an apparent spectral cutoff due to the bunch width of emitting electrons at $\omega \ll \omega_\gamma$. Rather than assuming a Gaussian electron distribution, which leads to an exponential falloff, we observe, as for thin foils, that the bunch has a sharp leading edge, leading to $10/3$ scaling for $T_L/t_b \ll \omega/\omega_L \ll \omega_\gamma/\omega_L$ [Fig. 5(a)], where t_b is the bunch duration [Fig. 5(b)]. The spectral transition can be seen in Fig. 5(a) around $\omega/\omega_L = 200$, well below the $\omega_\gamma/\omega_L = 7400$ cutoff expected from the observed $\gamma_z = 8.3$ and $\alpha_1 = 21$, but corresponding to a 2-nm bunch width. For ultrathin targets the bunch duration is much longer ($t_b/T_L \approx 0.5$) than for efficient semi-infinite interactions ($t_b/T_L \approx 0.002$), but the peak Lorentz factors are a much higher fraction of a_0: $(\gamma - 1)/a_0 \approx 0.3$ rather than 0.06. The difference in electron trajectories between the two cases results from the different electric fields experienced by emitting electrons. For thin foils the laser is partially transmitted, so the field is nonzero over the entire interaction region and even electrons with large longitudinal displacements are accelerated. The laser is entirely reflected for semi-infinite targets, with its field strength rapidly approaching zero within the plasma; electrons more than a few fractions of a wavelength from the surface are not accelerated. The electron bunch size is therefore larger in the ultrathin foil case and, since

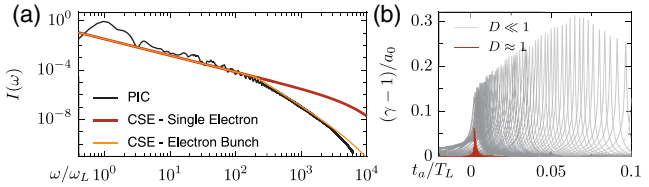

FIG. 5. (a) PIC spectrum of emission from a semi-infinite target with $a_0 = 100$, $N = 500$, and $\theta_L = 30°$. Spectral fits based on CSE scaling and the observed γ_z are provided uncorrected (red) and corrected (orange) for the bunch width. (b) Electron emission width ($0.002T_L$) compared to the thin-foil interaction in Fig. 2 ($0.5T_L$).

the reflected field is smaller and does not cancel the incident field at the target surface, the transverse acceleration is larger, leading to higher γ/a_0.

In conclusion, we have provided a general model for the spectrum of reflected emission produced by relativistic harmonic generation from ultrathin foils and shown that, with minor deviations, spectra for $D \ll 1$ follow $I(\omega) \propto \omega^{-10/3}$ up to the Lorentz-factor-dependent cutoff, which lies at higher frequencies than for thicker targets. This scaling is superior to that for moderate values of a_0 on solid-density thick targets but lower than the most efficient solid-target interactions, suggesting that where only moderate intensities are available, ultrathin foils provide an efficient source of relativistic high-order harmonics.

This work was partially supported by the National Science Foundation under Grants No. PHY 1506372 and No. PHY 1806911 and the Department of Energy under Grant No. DE-SC0017907. M. R. E. was partially supported by a Lawrence Fellowship with Project No. 20-ERD-057 from Lawrence Livermore National Laboratory. Simulations were performed at the High Performance Computing Center at Princeton University. The EPOCH code was developed as part of the UK EPSRC 300 360 funded Project No. EP/G054940/1. We would like to thank Paul Gibbon for help with the BOPS code. Lawrence Livermore National Laboratory is operated by Lawrence Livermore National Security, LLC, for the U.S. Department of Energy, National Nuclear Security Administration under Contract No. DE-AC52-07NA27344.

*edwards78@llnl.gov
†j.mikhailova@princeton.edu

[1] P. Gibbon, Harmonic Generation by Femtosecond Laser-Solid Interaction: A Coherent Water-Window Light Source?, Phys. Rev. Lett. **76**, 50 (1996).
[2] R. Lichters, J. Meyer-ter-Vehn, and A. Pukhov, Short-pulse laser harmonics from oscillating plasma surfaces driven at relativistic intensity, Phys. Plasmas **3**, 3425 (1996).
[3] S. Gordienko, A. Pukhov, O. Shorokhov, and T. Baeva, Relativistic Doppler Effect: Universal Spectra and Zeptosecond Pulses, Phys. Rev. Lett. **93**, 115002 (2004).
[4] N. M. Naumova, J. A. Nees, I. V. Sokolov, B. Hou, and G. A. Mourou, Relativistic Generation of Isolated Attosecond Pulses in a λ^3 Focal Volume, Phys. Rev. Lett. **92**, 063902 (2004).
[5] T. Baeva, S. Gordienko, and A. Pukhov, Theory of high-order harmonic generation in relativistic laser interaction with overdense plasma, Phys. Rev. E **74**, 046404 (2006).
[6] B. Dromey, M. Zepf, A. Gopal, K. Lancaster, M. Wei, K. Krushelnick, M. Tatarakis, N. Vakakis, S. Moustaizis, R. Kodama, M. Tampo, C. Stoeckl, R. Clarke, H. Habara, D. Neely, S. Karsch, and P. Norreys, High harmonic generation in the relativistic limit, Nat. Phys. **2**, 456 (2006).
[7] A. Tarasevitch, K. Lobov, C. Wünsche, and D. von der Linde, Transition to the Relativistic Regime in High Order Harmonic Generation, Phys. Rev. Lett. **98**, 103902 (2007).
[8] P. Heissler, A. Barna, J. M. Mikhailova, G. Ma, K. Khrennikov, S. Karsch, L. Veisz, I. Földes, and G. D. Tsakiris, Multi-μJ harmonic emission energy from laser-driven plasma, Appl. Phys. B **118**, 195 (2015).
[9] U. Teubner and P. Gibbon, High-order harmonics from laser-irradiated plasma surfaces, Rev. Mod. Phys. **81**, 445 (2009).
[10] F. Krausz and M. Ivanov, Attosecond physics, Rev. Mod. Phys. **81**, 163 (2009).
[11] S. X. Hu and L. A. Collins, Attosecond Pump Probe: Exploring Ultrafast Electron Motion Inside an Atom, Phys. Rev. Lett. **96**, 073004 (2006).
[12] D. an der Brügge and A. Pukhov, Enhanced relativistic harmonics by electron nanobunching, Phys. Plasmas **17**, 033110 (2010).
[13] J. M. Mikhailova, M. V. Fedorov, N. Karpowicz, P. Gibbon, V. T. Platonenko, A. M. Zheltikov, and F. Krausz, Isolated Attosecond Pulses from Laser-Driven Synchrotron Radiation, Phys. Rev. Lett. **109**, 245005 (2012).
[14] M. Behmke, D. an der Brügge, C. Rödel, M. Cerchez, D. Hemmers, M. Heyer, O. Jäckel, M. Kübel, G. Paulus, G. Pretzler, A. Pukhov, M. Toncian, T. Tonican, and O. Willi, Controlling the Spacing of Attosecond Pulse Trains from Relativistic Surface Plasmas, Phys. Rev. Lett. **106**, 185002 (2011).
[15] C. Rödel *et al.*, Harmonic Generation from Relativistic Plasma Surfaces in Ultrasteep Plasma Density Gradients, Phys. Rev. Lett. **109**, 125002 (2012).
[16] S. Kahaly, S. Monchocé, H. Vincenti, T. Dzelzainis, B. Dromey, M. Zepf, Ph. Martin, and F. Quéré, Direct Observation of Density-Gradient Effects in Harmonic Generation from Plasma Mirrors, Phys. Rev. Lett. **110**, 175001 (2013).
[17] F. Dollar, P. Cummings, V. Chvykov, L. Willingale, M. Vargas, V. Yanovsky, C. Zulick, A. Maksimchuk, A. G. R. Thomas, and K. Krushelnick, Scaling High-Order Harmonic Generation from Laser-Solid Interactions to Ultrahigh Intensity, Phys. Rev. Lett. **110**, 175002 (2013).
[18] C. Thaury and F. Quéré, High-order harmonic and attosecond pulse generation on plasma mirrors: Basic mechanisms, J. Phys. B **43**, 213001 (2010).
[19] A. A. Gonoskov, A. V. Korzhimanov, A. V. Kim, M. Marklund, and A. M. Sergeev, Ultrarelativistic nanoplasmonics as a route towards extreme-intensity attosecond pulses, Phys. Rev. E **84**, 046403 (2011).

[20] M. R. Edwards, V. T. Platonenko, and J. M. Mikhailova, Enhanced attosecond bursts of relativistic high-order harmonics driven by two-color fields, Opt. Lett. **39**, 6823 (2014).
[21] M. R. Edwards and J. M. Mikhailova, Multipass relativistic high-order harmonic generation for intense attosecond pulses, Phys. Rev. A **93**, 023836 (2016).
[22] M. R. Edwards and J. M. Mikhailova, Waveform-Controlled Relativistic High-Order-Harmonic Generation, Phys. Rev. Lett. **117**, 125001 (2016).
[23] M. Yeung, S. Rykovanov, J. Bierbach, L. Li, E. Eckner, S. Kuschel, A. Woldegeorgis, C. Rödel, A. Sävert, G. Paulus, M. Coughlan, B. Dromey, and M. Zepf, Experimental observation of attosecond control over relativistic electron bunches with two-colour fields, Nat. Photonics **11**, 32 (2017).
[24] P. Heissler, R. Hörlein, J. M. Mikhailova, L. Waldecker, P. Tzallas, A. Buck, K. Schmid, C. M. S. Sears, F. Krausz, L. Veisz, M. Zepf, and G. D. Tsakiris, Few-Cycle Driven Relativistically Oscillating Plasma Mirrors: A Source of Intense Isolated Attosecond Pulses, Phys. Rev. Lett. **108**, 235003 (2012).
[25] M. Yeung, B. Dromey, S. Cousens, T. Dzelzainis, D. Kiefer, J. Schreiber, J. H. Bin, W. Ma, C. Kreuzer, J. Meyer-ter-Vehn, M. J. V. Streeter, P. S. Foster, S. Rykovanov, and M. Zepf, Dependence of Laser-Driven Coherent Synchrotron Emission Efficiency on Pulse Ellipticity and Implications for Polarization Gating, Phys. Rev. Lett. **112**, 123902 (2014).
[26] A. Debayle, J. Sanz, and L. Gremillet, Self-consistent theory of high-order harmonic generation by relativistic plasma mirror, Phys. Rev. E **92**, 053108 (2015).
[27] M. Cherednychek and A. Pukhov, Analytical approach to high harmonics spectrum in the nanobunching regime, Phys. Plasmas **23**, 103301 (2016).
[28] H. Vincenti, Achieving Extreme Light Intensities Using Optically Curved Relativistic Plasma Mirrors, Phys. Rev. Lett. **123**, 105001 (2019).
[29] M. R. Edwards and J. M. Mikhailova, The x-ray emission effectiveness of plasma mirrors: Reexamining power-law scaling for relativistic high-order harmonic generation, Sci. Rep. **10**, 1 (2020).
[30] P. Gibbon, D. Altenbernd, U. Teubner, E. Förster, P. Audebert, J.-P. Geindre, J.-C. Gauthier, and A. Mysyrowicz, Plasma density determination by transmission of laser-generated surface harmonics, Phys. Rev. E **55**, R6352 (1997).
[31] U. Teubner, K. Eidmann, U. Wagner, U. Andiel, F. Pisani, G. D. Tsakiris, K. Witte, J. Meyer-ter-Vehn, T. Schlegel, and E. Förster, Harmonic Emission from the Rear Side of Thin Overdense Foils Irradiated with Intense Ultrashort Laser Pulses, Phys. Rev. Lett. **92**, 185001 (2004).
[32] A. S. Pirozhkov, S. V. Bulanov, T. Z. Esirkepov, M. Mori, A. Sagisaka, and H. Daido, Attosecond pulse generation in the relativistic regime of the laser-foil interaction: The sliding mirror model, Phys. Plasmas **13**, 013107 (2006).
[33] K. Krushelnick, W. Rozmus, U. Wagner, F. N. Beg, S. G. Bochkarev, E. L. Clark, A. E. Dangor, R. G. Evans, A. Gopal, H. Habara, S. P. D. Mangles, P. A. Norreys, A. P. L. Robinson, M. Tatarakis, M. S. Wei, and M. Zepf, Effect of Relativistic Plasma on Extreme-Ultraviolet Harmonic Emission from Intense Laser-Matter Interactions, Phys. Rev. Lett. **100**, 125005 (2008).
[34] H. George, F. Quéré, C. Thaury, G. Bonnaud, and Ph. Martin, Mechanisms of forward laser harmonic emission from thin overdense plasmas, New J. Phys. **11**, 113028 (2009).
[35] I. Choi, I. J. Kim, K. Pae, K. Nam, C.-L. Lee, H. Yun, H. Kim, S. Lee, T. Yu, J. Sung, A. Pirozhkov, K. Ogura, S. Orimo, H. Daido, and J. Lee, Simultaneous generation of ions and high-order harmonics from thin conjugated polymer foil irradiated with ultrahigh contrast laser, Appl. Phys. Lett. **99**, 181501 (2011).
[36] B. Dromey, S. Rykovanov, M. Yeung, R. Hörlein, D. Jung, D. Gautier, T. Dzelzainis, D. Kiefer, S. Palaniyppan, R. Shah, J. Schreiber, H. Ruhl, J. C. Fernandez, C. L. S. Lewis, M. Zepf, and B. M. Hegelich, Coherent synchrotron emission from electron nanobunches formed in relativistic laser-plasma interactions, Nat. Phys. **8**, 804 (2012).
[37] B. Dromey, S. Cousens, S. Rykovanov, M. Yeung, D. Jung, D. Gautier, T. Dzelzainis, D. Kiefer, S. Palaniyppan, R. Shah, J. Schreiber, J. C. Fernandez, C. L. S. Lewis, M. Zepf, and B. M. Hegelich, Coherent synchrotron emission in transmission from ultrathin relativistic laser plasmas, New J. Phys. **15**, 015025 (2013).
[38] S. Cousens, B. Reville, B. Dromey, and M. Zepf, Temporal Structure of Attosecond Pulses from Laser-Driven Coherent Synchrotron Emission, Phys. Rev. Lett. **116**, 083901 (2016).
[39] Yu. M. Mikhailova, V. T. Platonenko, and S. Rykovanov, Generation of an attosecond x-ray pulse in a thin film irradiated by an ultrashort ultrarelativistic laser pulse, JETP Lett. **81**, 571 (2005).
[40] J. M. Mikhailova and V. T. Platonenko, Efficient generation of attosecond xray radiation under interaction of ultra-relativistic few cycle laser pulse with a thin foil, AIP Conf. Proc. **827**, 429 (2006).
[41] R. Hörlein, S. Steinke, A. Henig, S. G. Rykovanov, M. Schnrer, T. Sokollik, D. Kiefer, D. Jung, X. Q. Yan, T. Tajima, J. Schreiber, M. Hegelich, P. V. Nickles, M. Zepf, G. D. Tsakiris, W. Sandner, and D. Habs, Dynamics of nanometer-scale foil targets irradiated with relativistically intense laser pulses, Laser Part. Beams **29**, 383 (2011).
[42] D. Kiefer, M. Yeung, T. Dzelzainis, P. Foster, S. Rykovanov, C. Lewis, R. Marjoribanks, H. Ruhl, D. Habs, J. Schreiber, M. Zepf, and B. Dromey, Relativistic electron mirrors from nanoscale foils for coherent frequency upshift to the extreme ultraviolet, Nat. Commun. **4**, 1763 (2013).
[43] J. Braenzel, A. A. Andreev, K. Y. Platonov, L. Ehrentraut, and M. Schnürer, Amplification of coherent synchrotron high harmonic emission from ultra-thin foils in relativistic light fields, Phys. Plasmas **24**, 080704 (2017).
[44] S. Gordienko and A. Pukhov, Scalings for ultrarelativistic laser plasma and quasimonoenergetic electrons, Phys. Plasmas **12**, 043109 (2005).
[45] V. A. Vshivkov, N. M. Naumova, F. Pegoraro, and S. V. Bulanov, Nonlinear electrodynamics of the interaction of ultra-intense laser pulses with a thin foil, Phys. Plasmas **5**, 2727 (1998).
[46] P. Gibbon, A. Andreev, E. Lefebvre, G. Bonnaud, H. Ruhl, J. Delettrez, and A. Bell, Calibration of one-dimensional

boosted kinetic codes for modeling high-intensity laser–solid interactions, Phys. Plasmas **6**, 947 (1999).

[47] T. D. Arber, K. Bennett, C. S. Brady, A. Lawrence-Douglas, M. G. Ramsay, N. J. Sircombe, P. Gillies, R. G. Evans, H. Schmitz, A. R. Bell, and C. P. Ridgers, Contemporary particle-in-cell approach to laser-plasma modelling, Plasma Phys. Controlled Fusion **57**, 113001 (2015).

[48] See the Supplemental Material at http://link.aps.org/supplemental/10.1103/PhysRevLett.124.185004 for details on computations, longer pulse durations, and multidimensional effects, which includes Ref. [49].

[49] A. Bourdier, Oblique incidence of a strong electromagnetic wave on a cold inhomogeneous electron plasma. Relativistic effects, Phys. Fluids **26**, 1804 (1983).

[50] V. Bratman and S. Samsonov, Radiation and radiative damping of a charged plane, oscillating with a relativistic velocity, Phys. Lett. A **206**, 377 (1995).